INTERNATIONAL JOURNAL OF
NUMERICAL ANALYSIS AND MODELING
Volume 10, Number 2, Pages 466–480

HIERARCHICAL A POSTERIORI RESIDUAL BASED ERROR ESTIMATORS FOR BILINEAR FINITE ELEMENTS

MALTE BRAACK AND NICO TASCHENBERGER

Abstract. We present techniques of a posteriori error estimation for Q_1 finite element discretizations based on residual evaluations with respect to test functions of higher-order. This technique is designed for quadrilateral (or hexahedral) triangulations and gives local error indicators in terms of nodal contributions. We show reliability and efficiency of the estimator. Moreover, we present a simplification which is attractive from computational point of view as well.

Key words. error estimates, adaptivity, finite elements

1. Introduction

The use of locally refined meshes for the numerical solution of partial differential equations may lead to efficient numerical methods. In adaptive algorithms, an important issue is the a posteriori error estimation and the extraction of local error indicators in order to decide which cells have to be refined.

The technique of a posteriori error estimation for finite element discretizations goes back to Babuška and Rheinboldt [3]. Since then, several alternative approaches have been proposed and analyzed, e.g., residual based indicators [1], and hierarchical estimators [4, 12]. Moreover, we like to refer the reader to the books of Ainsworth and Oden [2] and of Babuška and Strouboulis [10] for an overview of different techniques. An important step for a posteriori error estimation is the work of Verfürth [11] because it was not only shown that the proposed estimator is reliable but also efficient, i.e. the estimator can be bounded by the discretitzation error multiplied by a mesh size independent constant.

In this work, we propose a posteriori error estimators for bilinear finite elements which are based on the evaluation of residuals with respect to test functions of higher-order (bi-quadratic). In relation to the standard estimators of [11], we show that these estimators are locally equivalent. From the practical point of view, the estimator has the advantage that the computation of jump terms are not necessary. This is in particular advantageous on quadrilateral meshes with hanging nodes.

A second version of the estimator is even more attractive because it is cheaper in terms of numerical costs. We show the relation of this technique to established numerical techniques of dual weighted residuals (DWR). Some numerical examples illustrate the practical behaviour and show the reliability and efficiency.

The paper is structured as follows. In section 2, we formulate the Poisson problem and its discretization by finite elements. We recall the a posteriori error estimator proposed in [11]. In section 3, the hierarchical estimator is introduced and the relation to the estimator of the previous section is discussed. Moreover, we address shortly the relation to the implicit estimator of [3]. The modified and cheaper version is described in section 4. The basic idea is to use a coarser mesh for the

Received by the editors October 6, 2011 and, in revised form, April 20, 2012.
2000 *Mathematics Subject Classification.* 65N15, 65N30.
This work is partially supported by the DFG Priority Program SPP 1276 (MetStröm). This support is gratefully acknowledged.

evaluation of the residuals. The last section is devoted to some numerical examples in2D and 3D.

2. The model problem and its discretization

2.1. Variational formulation of the Poisson problem. We consider the Poisson problem with homogeneous Dirichlet boundary conditions in a two-dimensional polygonal domain $\Omega \subset \mathbb{R}^2$:

$$-\Delta u \;=\; f \text{ in } \Omega \quad \text{and} \quad u \,=\, 0 \text{ on } \partial\Omega\,. \tag{1}$$

All results carry over to mixed Dirichlet-Neumann conditions with the usual modifications.

In order to formulate the variational formulation we use the standard notations: for any open subset $\omega \subset \Omega$ let $L^2(\omega)$ be the Lebesgue space of square-integrable functions over ω, and $H^k(\omega)$ the Sobolev space with weak derivatives up to order $k \in \mathbb{N}$. The corresponding norms are denoted by $\|\cdot\|_\omega$ and $\|\cdot\|_{k;\omega}$, respectively. The L^2-scalar product and norm is denoted by $(\cdot,\cdot)_\omega$ and $\|\cdot\|$, respectively. In the case $\omega = \Omega$, we simply use $\|\cdot\|$, $\|\cdot\|_k$ and $(\cdot,\cdot)$. Furthermore, the Hilbert space of H^1 functions with vanishing traces on the boundary is denoted by $V := H^1_0(\Omega) = \{\phi \in H^1(\Omega) : \phi = 0 \text{ a.e. on } \partial\Omega\}$.

In the variational formulation, we seek for given right hand side $f \in L^2(\Omega)$ the function $u \in V$ such that

$$(\nabla u, \nabla\phi) \;=\; (f,\phi) \qquad \forall \phi \in V\,.$$

Due to the Theorem of Riesz, there is always a unique solution.

2.2. Discretization with finite elements. Let $\{\mathcal{T}_h\}_{h>0}$ be a shape regular family of triangulations of Ω consisting of triangles or quadrilaterals (but not both at the same time). For given h and $T \in \mathcal{T}_h$, h_T and ρ_T denote the diameter and the inner radius of T, respectively. The set of internal edges of $\mathcal{T}_h$ will be denoted by $\mathcal{E}_h$, i.e. for each edge $e \in \mathcal{E}_h$ the intersection $e \cap \partial\Omega$ does contain at most two boundary points. The shape regularity implies that the diameters $h_T, h_{T'}$ of two neighbouring cells $T, T' \in \mathcal{T}_h$ and the length h_e of a neighbouring edge e scale similar up to a h-independent constant:

$$0 \;<\; \max\{h_T, h_{T'}, h_e\} \;\leq\; c\min\{h_T, h_{T'}, h_e\}\,.$$

For triangular meshes, we use the space of polynomials up to degree r, denoted by $\mathcal{P}_r$. For quadrilateral meshes, the space of polynomials up to total degree r, denoted by $\mathcal{Q}_r$, is used. The finite element space is

$$\begin{aligned} \text{for tri's:}\quad V_h^{(r)} &:= \{\phi \in V : \phi|_T \in \mathcal{P}_r\,, \forall T \subset \mathcal{T}_h\}\,,\\ \text{for quad's:}\quad V_h^{(r)} &:= \{\phi \in V : \phi|_T \in \mathcal{Q}_r\,, \forall T \subset \mathcal{T}_h\}\,. \end{aligned}$$

The space of (bi-)linear elements is simply denoted by $V_h := V_h^{(1)}$. The space of piece-wise constant function is denoted by $V_h^{(0)}$.

With these notations, the corresponding finite element formulation reads

$$u_h \in V_h : \qquad (\nabla u_h, \nabla\phi) = (f,\phi) \quad \forall \phi \in V_h\,. \tag{2}$$

2.3. Standard a posteriori energy error estimate. For the formulation of the standard a posteriori energy error estimate of [11] we use the notation $\pi_h : L^2(\Omega) \to V_h^{(0)}$ for the L^2-projection, and $[v]_e$ for the jump of a cell-wise polynomial v across an edge e of $\mathcal{T}_h$. For edges e on the (Dirichlet) boundary, we make the convention $[v]_e := 0$. The cell-wise error contribution for $T \in \mathcal{T}_h$ consists of a cell residual and a jump term,

$$\theta_T \quad := \quad \left(h_T^2 \|\pi_h f + \Delta u_h\|_T^2 + h_T \|[\partial_n u_h]\|_{\partial T}^2\right)^{1/2} .$$

The energy error estimator reads (c.f. [11])

$$\theta \quad := \quad \left(\sum_{T \in \mathcal{T}_h} \theta_T^2 \right)^{1/2} . \tag{3}$$

We use the notation ω_T for a patch of cells $T' \in \mathcal{T}_h$ having at least one edge in common with T.

Theorem 1 (Verfürth, 1994)**.** *There are constants c_1, c_2 depending only on the polynomial degree r and the shape regularity of the family $\{\mathcal{T}_h\}_{h>0}$ such that*

$$\|\nabla(u - u_h)\|^2 \quad \leq \quad c_1 \left(\theta^2 + \sum_{T \in \mathcal{T}_h} h_T^2 \|f - \pi_h f\|_T^2 \right) ,$$

and for all $T \in \mathcal{T}_h$:

$$\theta_T^2 \quad \leq \quad c_2 \left(\|\nabla(u - u_h)\|_{\omega_T}^2 + h_T^2 \|f - \pi_h f\|_{\omega_T}^2 \right) .$$

If the discrete solution u_h is known, the local error indicators θ_T can be computed and used for local mesh refinement. According to Carstensen and Verfuerth [7], the two contributions of θ_T (the cell residual and the jump of the derivatives) are not equilibrated. For instance, for low-order finite elements (linear or bilinear), the jump term dominates the cell residual term. Further papers discussing this topic are given by Yu [13, 14] and in [12].

3. An error estimator based on higher-order residuals

We present an alternative approach for designing local error indicators for quadrilateral meshes. These error indicators are related to the degrees of freedom and not to the cells. We restrict here to $r = 1$ on quadrilateral meshes, so that the degrees of freedom are directly related to the inner nodes of the mesh. The construction takes advantage of the hierarchical basis of $V_h^{(r+1)}$ and is related to the approach on triangular meshes in [12]. We refer to Bank [4] for further benefits of hierarchical bases for finite elements.

3.1. Construction. By $\mathcal{N}_h$ we denote all inner nodes of $\mathcal{T}_h$, i.e., those nodes which are not located on the (Dirichlet) boundary $\partial\Omega$. It holds $n_h := |\mathcal{N}_h| = \dim V_h$. $\mathcal{B}_h^{(1)} := \{\psi_1, \ldots, \psi_{n_h}\}$ denotes the Lagrangian nodal basis of V_h. Each ψ_i is a standard 'hat-function' corresponding to a node $N_i \in \mathcal{N}_h$.

In order to build a basis $\mathcal{B}_h^{(2)}$ of $V_h^{(2)}$, the bi-quadratic finite elements, we consider the mesh $\mathcal{T}_{h/2}$ which arises by one global refinement of $\mathcal{T}_h$. We divide the nodes of $\mathcal{N}_{h/2}$ in three types,

$$\mathcal{N}_{h/2} \quad = \quad \mathcal{N}_h \cup \mathcal{N}_{h/2}^E \cup \mathcal{N}_{h/2}^C ,$$

where $\mathcal{N}_{h/2}^E$ consists of nodes located on inner edges of $\mathcal{T}_h$, and $\mathcal{N}_{h/2}^C$ consists of nodes located on cell centers of $\mathcal{T}_h$. Hence, $|\mathcal{N}_{h/2}^E| = |\mathcal{E}_h|$ and $|\mathcal{N}_{h/2}^C| = |\mathcal{T}_h|$. We fix

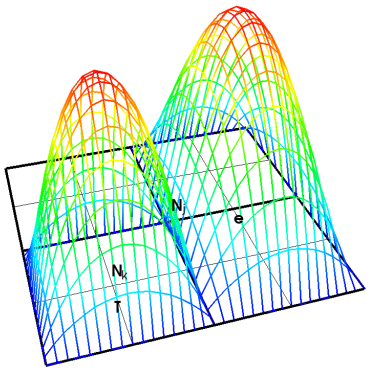

FIGURE 1. Cell-bubble function ψ_T (left bulb) and edge-bubble function ψ_e (right bulb).

a numbering of the nodes of $\mathcal{N}_{h/2}$. Now, the hierarchical basis $\mathcal{B}_h^{(2)}$ consists of the hat-functions $\psi \in \mathcal{B}_h^{(1)}$, edge bubbles ψ_e, and cell bubbles ψ_T,

$$\mathcal{B}_h^{(2)} \quad := \quad \mathcal{B}_h^{(1)} \cup \{\psi_e : e \in \mathcal{E}_h\} \cup \{\psi_T : T \in \mathcal{T}_h\}\,.$$

In Figure 1, a cell-bubble and an edge-bubble function is illustrated. This leads to a canonical bijective mapping between the indices and this quadratic basis,

$$\psi^{(2)} : \{1, \ldots, n_{h/2}\} \to \mathcal{B}_h^{(2)}\,, \quad k \mapsto \psi_k^{(2)}\,,$$

which corresponds to the numbering of the nodes of $\mathcal{N}_{h/2}$. This means, if $k \in \mathcal{N}_{h/2}^C$, then $\psi_k^{(2)}$ is the cell bubble function centered at N_k; if $k \in \mathcal{N}_{h/2}^E$, then $\psi_k^{(2)}$ is the edge bubble function centered at the node N_k. For each of these indices $1 \le i \le n_{h/2}$, we define the residual corresponding to this quadratic basis,

$$\Psi_i \quad := \quad (\pi_h f, \psi_i^{(2)}) - (\nabla u_h, \nabla \psi_i^{(2)})\,. \tag{4}$$

The absolute values of these residuals will be our local error indicators

$$\eta_i \quad := \quad |\Psi_i|\,, \tag{5}$$

and their sum will be the a posteriori error estimator

$$\eta \quad := \quad \left(\sum_{i=1}^{n_{h/2}} \eta_i^2 \right)^{1/2}\,. \tag{6}$$

Hence, instead of evaluating jump terms, the estimator just consists in computing residuals to higher-order test functions.

3.2. Locally equivalence of the error estimators. We will show that the cell error indicators (3) and the nodal based ones (5) are "locally equivalent" in the sense of Dörfler [8]. For this we need some preparatory results.

Lemma 2. *Let $\{\mathcal{T}_h\}$ be a quasi-uniform family of triangulations consisting of parallelogram meshes. For $N_k \in \mathcal{N}_{h/2}^C$ let $T \in \mathcal{T}_{h/2}$ be the corresponding cell (i.e. $N_k \in T \setminus \partial T$). There are constants $c_1, c_2 > 0$ so that*

$$c_1|\Psi_k| \quad \le \quad h_T \|\pi_h f + \Delta u_h\|_T \quad \le \quad c_2|\Psi_k|\,.$$

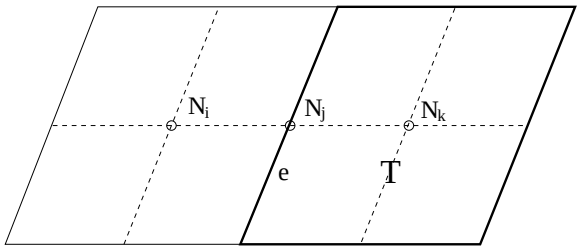

FIGURE 2. Nodes for the quadratic bubble functions in the proof of the Lemmata.

Proof. The L^2-projected right hand side $\pi_h f$ is constant on T. We use the abbreviation f_T for the L^2-projected right hand side, $f_T = \pi_h f|_T$. Since T is a parallelogram, Δu_h is constant on T (for rectangulars it even vanishes). Therefore, we may set $g_T := (\pi_h f + \Delta u_h)|_T$. On the one hand, we obtain for the residual

$$\begin{aligned} |\Psi_k| &= |(\pi_h f + \Delta u_h, \psi_k^{(2)})| = (|g_T|, \psi_k^{(2)}) = |g_T| \int_T \psi_k^{(2)}\, dx \\ &= |g_T||T| \int_{\widehat{T}} \widehat{\psi}^{(2)}\, d\widehat{x}\,. \end{aligned}$$

On the other hand it holds

$$h_T \|\pi_h f + \Delta u_h\|_T = |g_T| h_T |T|^{1/2}\,.$$

Due to

$$c_2^{-1} h_T \leq |T|^{1/2} \int_{\widehat{T}} \widehat{\psi}^{(2)}\, d\widehat{x} \leq c_1^{-1} h_T\,,$$

with appropriate constants $c_1, c_2 > 0$, we obtain the assertion. □

Lemma 3. *Let $\{\mathcal{T}_h\}$ be a quasi-uniform family of triangulations consisting of parallelogram meshes. For $N_j \in \mathcal{N}_{h/2}^E$ on an edge $e \in \mathcal{E}_h$ let $N_i, N_k \in \mathcal{N}_{h/2}^C$ be the nodes of the adjacent cell bubble functions* (see Figure 2). *There is a constant $c > 0$ so that*

$$h_e^{1/2} \|[\partial_n u_h]\|_e \leq c(|\Psi_i| + |\Psi_j| + |\Psi_k|)\,.$$

Proof. Since the L_2-norm and a weighted L_1-norm are equivalent in a finite dimensional space, it holds on a reference edge $\widehat{e}$ for arbitrary linear functions $\widehat{v}$:

$$\|\widehat{v}\|_{\widehat{e}} \leq c \int_{\widehat{e}} |\widehat{v}| \widehat{\psi}\,,$$

where $\widehat{\psi}$ is the reference bubble function on $\widehat{e}$. By a scaling argument we get on the edge e with the edge bubble function $\psi_j^{(2)}$

$$h_e^{1/2} \|v\|_e = h_e \|\widehat{v}\|_{\widehat{e}} \leq c h_e \int_{\widehat{e}} |\widehat{v}| \widehat{\psi} = c \int_e |v| \psi_j^{(2)}\,,$$

and in particular

$$h_e^{1/2} \|[\partial_n u_h]\|_e \leq c \left| \int_e [\partial_n u_h] \psi_j^{(2)} \right|\,.$$

We denote the two cells supporting $\psi_i^{(2)}$ and $\psi_k^{(2)}$ by $T_i, T_k \in \mathcal{T}_h$, respectively. Due to $\mathrm{supp}(\psi_j^{(2)}) = T_i \cup T_k$, we get by Green's formula

$$\begin{aligned} h_e^{1/2}\|[\partial_n u_h]\|_e &\leq c|(\nabla u_h, \nabla\psi_j^{(2)})| = c|(\pi_h f + \Delta u_h, \psi_j^{(2)}) - \Psi_j| \\ &\leq c(\|\pi_h f + \Delta u_h\|_{T_i\cup T_k}\|\psi_j^{(2)}\| + |\Psi_j|) \\ &\leq c(\|\pi_h f + \Delta u_h\|_{T_i\cup T_k}|T_i \cup T_k|^{1/2} + |\Psi_j|)\,. \end{aligned}$$

Noting that $|T_i \cup T_k| \leq h_i^2 + h_k^2 \leq c h_e^2$ and applying Lemma 2, we get the assertion. □

Lemma 4. *Let $\{\mathcal{T}_h\}$ be a quasi-uniform family of triangulations consisting of parallelogram meshes. Let $N_j \in \mathcal{N}_{h/2}^E$ be the node on the edge $e \in \mathcal{E}_h$. The two adjacent cells of e are denoted by $T_i, T_k \in \mathcal{T}_h$. Then it holds with a constant $c > 0$:*

$$|\Psi_j| \leq c\left(h_{T_i}\|\pi_h f + \Delta u_h\|_{T_i\cup T_k} + h_e^{1/2}\|[\partial_n u_h]\|_e\right).$$

Proof.

$$\begin{aligned} |\Psi_j| &= |(\pi_h f, \psi_j^{(2)}) - (\nabla u_h, \nabla\psi_j^{(2)})| \\ &= \left|(\pi_h f + \Delta u_h, \psi_j^{(2)})_{T_i\cup T_k} + ([\partial_n u_h], \psi_j^{(2)})_e\right| \\ &\leq \|\pi_h f + \Delta u_h\|_{T_i\cup T_k}\|\psi_j^{(2)}\| + \|[\partial_n u_h]\|_e\|\psi_j^{(2)}\|_e \\ &\leq c((h_{T_i} + h_{T_k})\|\pi_h f + \Delta u_h\|_{T_i\cup T_k} + h_e^{1/2}\|[\partial_n u_h]\|_e)\,. \end{aligned}$$

The mesh sizes h_{T_i} and h_{T_j} are of similar size, so that $h_{T_i} + h_{T_j} \leq c h_{T_i}$. □

For each cell $T \in \mathcal{T}_h$, we define the set $I(T) \subset \{1, \ldots, n_{h/2}\}$ containing the indices of the corresponding "cell bubble" function and "edge bubble" functions; $|I(T)| \leq 5$. In the opposite way, for each node $N_i \in \mathcal{N}_{h/2}$, we define $T(i) \subset \mathcal{T}_h$, so that $T \in T(i)$ implies $N_i \in T$. We are now in the situation to show the local equivalence between θ and η.

Proposition 5. *Let $\{\mathcal{T}_h\}_{h>0}$ be a shape-regular family of parallelogram meshes. Then the cell based indicators (3) and the nodal based indicators (5) are locally equivalent, i.e.,*

$$0 \leq \eta_i \leq c \sum_{T\in T(i)} \theta_T \quad \text{and} \quad 0 \leq \theta_T \leq c \sum_{i\in I(T)} \eta_i\,, \tag{7}$$

with a constant $c > 0$ independent of h.

Proof. The estimates follow immediately from the previous three lemmata. □

As a consequence, we get a similar result as in Theorem 1 for η :

Proposition 6. *Let $\{\mathcal{T}_h\}_{h>0}$ be a shape-regular family of parallelogram meshes. Then it holds for the estimator given by (5) and (6)*

$$\|\nabla(u - u_h)\|^2 \leq c_1\left(\eta^2 + \sum_{T\in\mathcal{T}_h} h_T^2\|f - \pi_h f\|_T^2\right), \tag{8}$$

and for all $i \in \{1, \ldots, n_{h/2}\}$:

$$\eta_i \leq c_2\|\nabla(u - u_h)\|_{T(i)}\,. \tag{9}$$

Proof. The reliability bound (8) is a direct consequence of the previous proposition and Theorem 1. The efficiency bound (9) can not be derived by the previous Propositions due to the appearance of fluctuations in the right hand side, $\|f-\pi_h f\|_T$ in Theorem 1. Therefore, we use the criterion in [12] (Prop. 1.14 and 1.15) which is originally formulated for triangular meshes and P_1-elements but can easy be generalized to Q_1-elements on quadrilateral meshes. To this end, we observe that for each edge bubble function $\psi_e \in \mathcal{B}_h^{(2)}$ and all cell bubble basis functions $\psi_T \in \mathcal{B}_h^{(2)}$ it holds

$$0 \quad \leq \quad \psi_e, \psi_T \quad \leq \quad 1\,.$$

Furthermore, let $e \in \mathcal{E}_h$ be an inner edge and $T_i, T_k \in \mathcal{T}_h$ the adjacent cells. Then it is easy to verify by a simple scaling argument the following estimates for the corresponding edge bubble function $\psi_e \in \mathcal{B}_h^{(2)}$:

$$\begin{aligned} c_3 h_e &\leq \int_e \psi_e \, dx\,, \\ h_e \|\nabla \psi_e\|_{T_i \cup T_k} &\leq c_4 \|\psi_e\|_{T_i \cup T_k}\,. \end{aligned}$$

with $c_3 > 0$. Similarly, it holds for each cell bubble basis functions $\psi_T \in \mathcal{B}_h^{(2)}$:

$$\begin{aligned} c_3 h_T^2 &\leq \int_T \psi_T \, dx\,, \\ h_T \|\nabla \psi_T\|_T &\leq c_4 \|\psi_T\|_T\,. \end{aligned}$$

Now, the bound (9) follows by applying Prop. 1.14 and 1.15 of [12]. □

Remark 7. *The extension of this approach to three dimensions, $d = 3$, is possible. The analogous estimates of Lemma 2 and 3 become*

$$\begin{aligned} c_1 h_T^{-1/2} |\Psi_k| &\leq h_T \|\pi_h f + \Delta u_h\|_T \leq c_2 h_T^{-1/2} |\Psi_k|\,, \\ h_e^{1/2} \|[\partial_n u_h]\|_e &\leq c_2 h_T^{-1/2} (|\Psi_i| + |\Psi_j| + |\Psi_k|)\,. \end{aligned}$$

The local error indicators of the estimator η reads in three dimensions:

$$\eta_i \quad := \quad h_i^{-1/2} |\Psi_i|\,,$$

where h_i it the maximal diameter of all cells containing node N_i. Only basis function corresponding to cells and faces are needed. The basis functions corresponding to edges are not needed.

3.3. Relation to an implicit error estimator. The proposed estimator (6) has a certain relationship to the estimator proposed in [3], where the residuals Ψ_j enter as right-hand sides for local Poisson problems. For each node $N_j \in \mathcal{N}_h$, the corresponding patch $\omega_j := \bigcup_{T \in T(j)} T$ is considered, see Figure 3 for illustration. The solutions of the local problem in $W_j := V_h^{(2)} \cap H_0^1(\omega_j)$,

$$w_j \in W_j : \quad (\nabla w_j, \nabla \psi)_{\omega_j} \quad = \quad (\pi_h f, \psi)_{\omega_j} - (\nabla u_h, \nabla \psi)_{\omega_j} \quad \forall \psi \in W_j\,, \tag{10}$$

enter into the estimator of Babuška and Rheinboldt

$$\eta_{BR} \quad := \quad \left(\sum_{j=1}^{n_h} \|\nabla w_j\|^2 \right)^{1/2}\,.$$

In order to see the relation to (6) we consider the following set of indices,

$$I_j \quad := \quad \{1 \leq i \leq n_{h/2} : \, supp(\psi_i^{(2)}) \subset \omega_j\}\,.$$

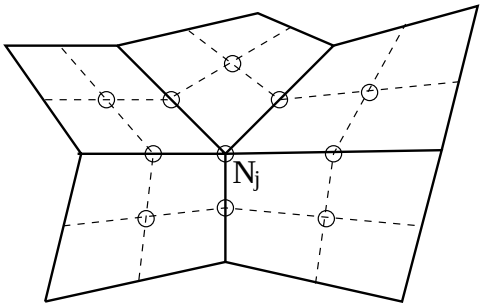

FIGURE 3. This patch ω_j includes 11 indices located in five cells of $\mathcal{T}_h$ around node N_j.

The local problem (10) can now be formulated as

$$w_j \in W_j : \quad (\nabla w_j, \nabla \psi_i^{(2)})_{\omega_j} \quad = \quad \Psi_i \quad \forall i \in I_j \, .$$

Let α_{ij}, $i \in I_j$, be the coefficients for the representation of w_j in the hierarchical quadratic basis,

$$w_j \quad = \quad \sum_{i \in I_j} \alpha_{ij} \psi_i^{(2)} \, .$$

Here, we used the fact $w_j \in \mathrm{span}\langle \psi_i^{(2)} \in \mathcal{B}_h^{(2)} : i \in I_j \rangle$. With these notations, we may express η_{BR} by a sum over the nodes of $\mathcal{N}_{h/2}$:

$$\eta_{BR}^2 \quad = \quad \sum_{j=1}^{n_h} \sum_{i \in I_j} \alpha_{ij} (\nabla w_j, \nabla \psi_i^{(2)}) = \sum_{j=1}^{n_h} \sum_{i \in I_j} \alpha_{ij} \Psi_i \, .$$

Using the index set $\widetilde{I}_i := \{ j \in \{1, \ldots, n_h\} | i \in I_j \}$ and the notation

$$\overline{\alpha}_i \quad := \quad \sum_{j \in \widetilde{I}_i} \alpha_{ij} \, ,$$

we arrive at

$$\eta_{BR} \quad = \quad \left(\sum_{i=1}^{n_{h/2}} \overline{\alpha}_i \Psi_i \right)^{1/2} \, .$$

Hence, η_{BR} can be expressed as weighted sum of residuals Ψ_i with coefficient $\overline{\alpha}_i$ determined by solving the auxiliary problems (10). In the particular case $\overline{\alpha}_i \approx \Psi_i$ for all i, the proposed estimator (6) is an approximation of the implicit estimator, $\eta_{BR} \approx \eta$. Therefore, (6) can be interpreted as an explicit variant of η_{BR} without solving local problems.

4. A cheaper variant on a coarser mesh

Although the proposed estimator (6) does not need the solution of local problems, the evaluation of residual terms for the higher-order test functions is more expensive than the residual of the lower-order test functions. For reducing the costs further, one may change the estimator by taking the higher-order residuals on a coarser mesh. For this we assume that the triangulation $\mathcal{T}_h$ is organized in a patch-wise manner, i.e., $\mathcal{T}_h$ results from a coarser locally refined mesh $\mathcal{T}_{2h}$ by one global refinement. An estimator can now be formulated as before, but with the difference that the quadratic test functions $\psi_i^{(2)}$ are chosen out of the space $V_{2h}^{(2)}$. Therefore,

only the nodes of $\mathcal{N}_h$, and hence much less quadratic test functions, are considered. We define

$$\Psi_i' := (\pi_h f, \psi_i^{(2)}) - (\nabla u_h, \nabla \psi_i^{(2)}), \quad \psi_i^{(2)} \in \mathcal{B}_{2h}^{(2)}, \tag{11}$$

$$\eta_i' := |\Psi_i'|, \tag{12}$$

$$\eta' := \left(\sum_{i=1}^{n_h} \eta_i'^2 \right)^{1/2}. \tag{13}$$

Note, that $\Psi_i' = 0$ if $N_i \in \mathcal{N}_{2h}$, because then $\psi_i^{(2)} \in V_h$ due to the hierarchical construction of the basis. The local indicators η_i' can be bounded from above by η_i:

Proposition 8. *There exists a constant $c > 0$ with*

$$\eta_i' \leq c \sum_{j \in I_i} \eta_j \leq c \left(\|\nabla(u - u_h)\|_{T(i)}^2 + \sum_{T \in T(i)} h_T^2 \|f - \pi_h f\|_T^2 \right)^{1/2}.$$

Proof. Since $V_{2h}^{(2)} \subset V_h^{(2)}$, the quadratic test function $\psi_i^{(2)} \in \mathcal{B}_{2h}^{(2)}$ can be expressed by a linear combination of test functions in $\mathcal{B}_h^{(2)}$ with support in $T(i)$: In particular, there is a finite number of h-independent coefficients $\{\beta_{ji} : j \in I_j\}$ such that

$$\eta_i' = |\Psi_i'| = \left| \sum_{j \in I_i} \beta_{ji} \Psi_j \right| \leq \sum_{j \in I_i} |\beta_{ji}| \eta_j .$$

The second upper bound follows immediately from Proposition 6 and the fact that for $j \in I_i$, $T(j) \subset T(i)$. □

4.1. Relation to estimators of functional output. In order to measure the error of functional output, the dual-weighted residual (DWR) method of Becker & Rannacher [5] is widely established. To this end, we consider a (possibly nonlinear) variational equation of the form

$$u \in V : \quad \varrho(u, \phi) = 0 \quad \forall \phi \in V ,$$

with a semi-linear form $\varrho : V \times V \to \mathbb{R}$ which is linear in the second argument and Frechét differentible in the first argument. A possible error representation with respect to a functional $j : V \to \mathbb{R}$ is

$$j(u) - j(u_h) = \varrho(u_h, z - i_h z) + R ,$$

with a remainder R which is (formally) of second order in the error. Here, $z \in V$ is the solution of the corresponding adjoint problem

$$z \in V : \quad \varrho'(u_h)(\phi, z) = j'(u)(\phi) \quad \forall \phi \in V .$$

We approximate the interpolation error by a higher-order interpolation of the numerical approximation z_h,

$$z - i_h z \approx i_{2h}^{(2)} z_h - z_h ,$$

where $i_{2h}^{(2)}$ is the quadratic interpolation on the mesh $\mathcal{T}_{2h}$, i.e. $i_{2h}^{(2)} : V \to V_{2h}^{(2)}$. We obtain with the nodal values $Z_i := z_h(N_i)$,

$$i_{2h}^{(2)} z_h - z_h = \sum_{i=1}^{n_h} (\psi_i^{(2)} - \psi_i) Z_i .$$

Now, we express the estimator e.g. used in [6],

$$\sigma \quad := \quad \varrho(u_h, i_{2h}^{(2)} z_h - z_h)$$

in terms of the nodal fluctuations

$$Z_i^\pi \quad := \quad z_h(N_i) - (i_{2h}^h z_h)(N_i)$$

and the residuals Ψ' as follows:

$$\begin{aligned}
\sigma &= \varrho(u_h, i_{2h}^{(2)} z_h - i_{2h} z_h) + \varrho(u_h, i_{2h} z_h - z_h) \\
&= \varrho(u_h, i_{2h}^{(2)} z_h - i_{2h} z_h) \\
&= \sum_{i=1}^{n_h} \varrho(u_h, \psi_i^{(2)} - \psi_i) Z_i^\pi \\
&= \sum_{i=1}^{n_h} \varrho(u_h, \psi_i^{(2)}) Z_i^\pi \\
&= \sum_{i=1}^{n_h} \Psi_i' Z_i^\pi \,.
\end{aligned}$$

By Hölders inequality we obtain the upper bound including the estimator η':

$$\sigma \quad \le \quad \sum_{i=1}^{n_h} |\Psi_i Z_i^\pi| \;\le\; \left(\sum_{i=1}^{n_h} \Psi_i^2 \right)^{1/2} \left(\sum_{i=1}^{n_h} (Z_i^\pi)^2 \right)^{1/2} \;=\; \eta' \left(\sum_{i=1}^{n_h} (Z_i^\pi)^2 \right)^{1/2} .$$

In order to illustrate the relation to the proposed error indicators (13), we consider the Poisson problem (1) and the energy error. In this case the (nonlinear) functional becomes

$$j(u) \quad = \quad \|\nabla u\|^2 \,,$$

so that by Galerkin orthogonality

$$j(u) - j(u_h) \quad = \quad \|\nabla u\|^2 - \|\nabla u_h\|^2 = \|\nabla (u - u_h)\|^2 \,.$$

By help of an inverse estimate, the fluctuation coefficients Z_i^π can be approximated by the local L_2-error on the patch ω_i around the node N_i. We denote the local mesh size close to node N_i by h_i,

$$|Z_i^\pi| \quad \le \quad c h_i^{-d/2} \|z_h - i_{2h}^h z_h\|_{\omega_i} \,.$$

For quasi uniform meshes with the maximal mesh size h, the sum can be approximated by the interpolation error by

$$\begin{aligned}
\left(\sum_{i=1}^{n_h} (Z_i^\pi)^2 \right)^{1/2} &\le c \left(\sum_{i=1}^{n_h} h_i^{-d} \|z_h - i_{2h}^h z_h\|_{\omega_i}^2 \right)^{1/2} \\
&\le c h^{-1} \|z - i_h z\| \;\le\; c_i \|\nabla z\| \;\le\; c_i \,.
\end{aligned}$$

Because in the case of the energy error, the dual solution is equal to the error

$$z = \frac{u - u_h}{\|\nabla (u - u_h)\|} \,,$$

we have the a priori estimate $\|\nabla z\| \le 1$ and recover an upper bound of σ by the estimator (12):

$$\sigma \quad \le \quad c_i \left(\sum_{i=1}^{n} \Psi_i^2 \right)^{1/2} \;=\; c_i \eta' \,.$$

Hence, a possible reliablity of σ carries over to the reliablity of η'. In this case, η' becomes reliable and efficient.

5. Numerical tests

In this section, we perform numerical comparison between the following estimators:

- SEE: the **S**tandard **E**rror **E**stimator θ given by (3),
- HEE: the **H**igher order residual **E**rror **E**stimator η given by (6), and
- CEE: the **C**oarse mesh higher order residual **E**rror **E**stimator η' given by (13)

An important and established quality measure is the efficiency index

$$I_{eff}(\eta) = \frac{\eta}{\|\nabla(u - u_h)\|} .$$

We will use equidistant tensor meshes and local refined meshes. The algorithm to obtain latter onces is given in the next subsection.

5.1. Adaptive strategy. In order to compare the performance of the estimators under local mesh refinement we use the mesh adaption strategy described by Richter [9]. As usual for mesh adaptation, the cell-wise error indicators are assumed to be ordered

$$\eta_{K_i} \quad \geq \quad \eta_{K_{i+1}} .$$

The adaptation strategy determines an integer m which is the maximal cell index to be refined, i.e. $K_1,\ldots,K_m$ will be marked to be refined. The value of m is determined by considering the lowest value of the product of the expected error on the refined mesh and the corresponding numerical costs with a certain power. We refer to [9] for more details. The local refinement is done by the use of hanging nodes.

5.2. Two-dimensional L-shaped domain. We consider the L-shaped domain reported by Carstensen and Verführt [7], $\overline{\Omega} = [-1,1] \times [0,1] \cup [-1,0] \times [-1,0]$. The right-hand side is equal to one, $f \equiv 1$, and the boundary conditions are homogeneous Dirichlet conditions. Due to Galerkin orthogonality it holds

$$\|\nabla(u - u_h)\| \quad = \quad \sqrt{\|\nabla u\|^2 - \|\nabla u_h\|^2} . \tag{14}$$

The value $\|\nabla u\|^2$ is approximated numerically by a Q_2 solution on a very fine mesh with approximately three millions of cells, $\|\nabla u\| \approx e := 0.4626813$. It holds $|\|\nabla u\|^2 - e^2| \leq 10^{-5}$.

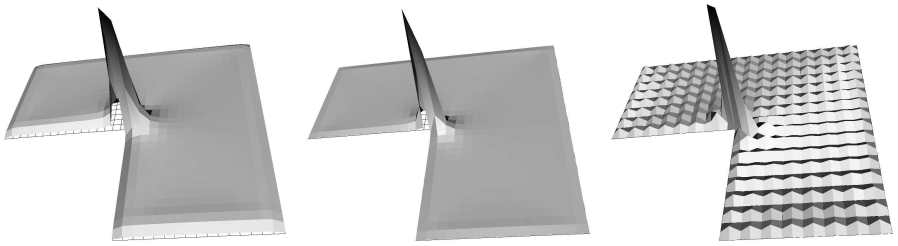

FIGURE 4. Local error indicators for SEE (left), HEE (middle) and CEE (right) for the L-shaped domain.

TABLE 1. Exact error and estimated errors on globally refined 2D meshes (L-shaped domain).

		SEE		HEE		CEE	
#nodes	$\|\nabla(u-u_h)\|$	θ	I_{eff}	η	I_{eff}	η'	I_{eff}
21	2.35e-01	1.26e+00	5.35	4.58e-01	1.95	2.06e-01	0.87
65	1.23e-01	6.72e-01	5.48	2.48e-01	2.02	1.19e-01	0.97
225	6.51e-02	3.51e-01	5.39	1.34e-01	2.06	6.51e-02	1.00
833	3.53e-02	1.81e-01	5.13	7.24e-02	2.05	3.52e-02	1.00
3,201	1.97e-02	9.35e-02	4.76	3.96e-02	2.02	1.90e-02	0.97
12,545	1.12e-02	4.85e-02	4.33	2.21e-02	1.97	1.03e-02	0.92
49,665	6.52e-03	2.55e-02	3.92	1.26e-02	1.93	5.71e-03	0.88
197,633	3.82e-03	1.37e-02	3.58	7.35e-03	1.93	3.23e-03	0.85

TABLE 2. Efficiency indices for local mesh refinement of L-shaped domain (2D).

SEE		HEE		CEE	
#nodes	$I_{eff}(\theta)$	#nodes	$I_{eff}(\eta)$	#nodes	$I_{eff}(\eta')$
225	5.39	225	2.06	225	0.94
833	5.13	385	2.10	833	0.94
3,201	4.76	1,169	2.13	3,201	0.91
3,537	5.61	3,737	2.13	3,861	1.00
13,513	5.36	4,073	2.21	13,377	0.98
13,985	6.03	14,493	2.20	14,925	1.06
53,057	6.00	14,953	2.26	53,285	1.06
53,801	6.50	55,521	2.31	57,329	1.13
54,497	6.71	56,181	2.36	210,397	1.23
212,477	7.71	216,693	2.67	224,957	1.32

Table 1 shows the results on globally refined meshes. The three variants provide reliable results. The efficiency of the standard error estimator is between 5.35 and 3.58 and is getting better on finer meshes. This results match the results in [7]. For HEE the efficiency is close to 2 for all meshes, CEE provides the best estimation and its efficiency index is always between 0.85 and 1.00. On finer meshes, the error is slightly underestimated.

The distributions of the error indicators are shown in Figure 4. The indicators of SEE and HEE are nearly the same. CEE exhibits the mentioned zero values at the coarse grid nodes $\mathcal{N}_{2h}$.

Several obtained locally refined meshes and zooms into the vicinity of the singularity are given in Figure 5. For all three indicators, the resulting meshes look pretty similar and show the typical 'cloverleaf' appearance.

The obtained efficiency indices are listed in Table 2. Also on locally refined meshes, all of them seem to be robust under mesh refinement. However, the cheap variant CEE delivers the best results again in the sense that they are closest to one.

We compare in Figure 6 the relation between n_h (number of degrees of freedom) and $\|\nabla(u-u_h)\|$ on globally refined meshes and on locally refined meshes obtained by these different estimators. In this context, the adaptive strategy outperforms local refinement independently of the type of estimator. But even though the estimated quantities differ, the resulting local refined meshes lead to the same convergence

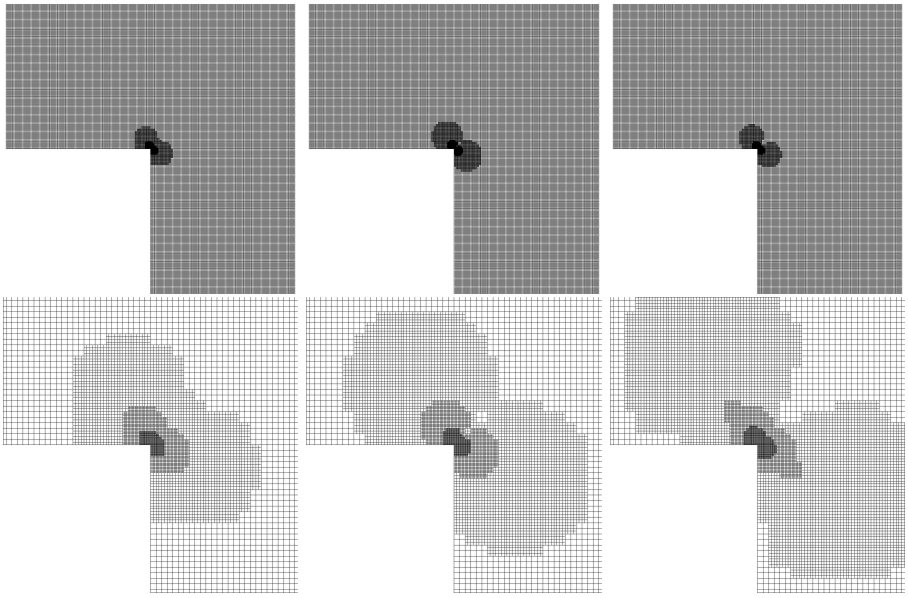

FIGURE 5. Local refined meshes for the L-shaped domain (2D). The upper row show the entire mesh for SEE (left), HEE (middle) and CEE (right). The lower row shows corresponding zooms around the singularity. All estimators give qualitatively very similar meshes.

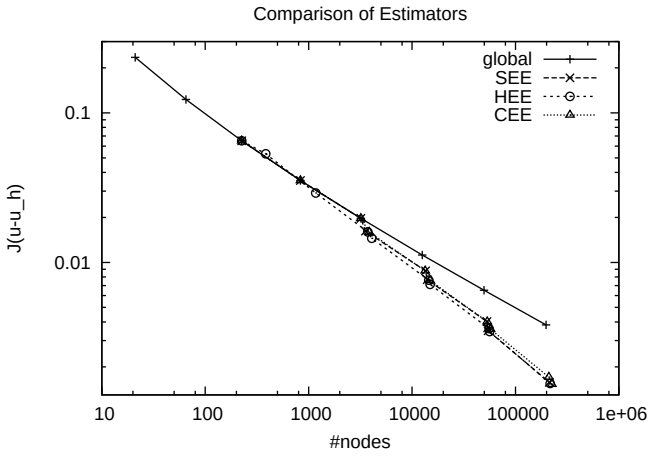

FIGURE 6. Comparison of performance of the different estimators on L-shaped domain (2D).

rates for all three error estimators. Note, that the curve of the standard estimator SEE is covered by the other curves.

5.3. Three-dimensional L-shaped domain. As a three-dimensional model problem we take $\Omega = (-1,1)^3 \setminus \{(0,1)^2 \times (-1,0)\}$, right hand side $f \equiv 1$ and homogeneous Dirichlet data. As before, the value $\|\nabla u\|^2$ is approximated numerically using Q_2 finite elements on a mesh with approximately 15 million cells. It is given by

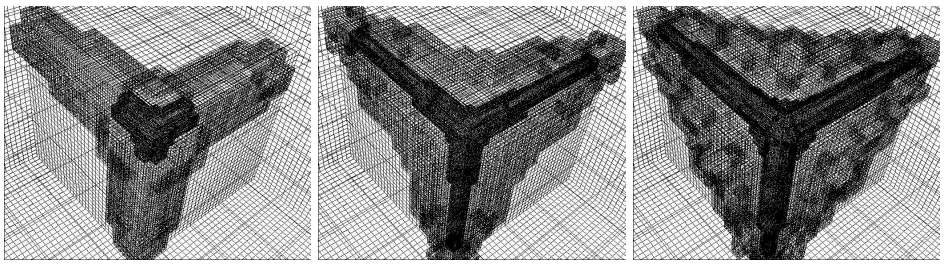

FIGURE 7. Cutouts of locally refined 3D meshes around the inner corner after four adaptive steps obtained with the estimator SEE (left), HEE (middle) and CEE (right).

TABLE 3. Obtained values in 3D with estimators SEE, HEE and CEE on globally refined meshes.

		SEE		HEE		CEE	
#nodes	$\|\nabla(u-u_h)\|$	θ	I_{eff}	η	I_{eff}	η'	I_{eff}
117	3.23e-01	1.83e+00	5.66	4.61e-01	1.43	2.29e-01	0.71
665	1.71e-01	1.00e+00	5.85	2.44e-01	1.43	1.14e-01	0.66
4401	9.17e-02	5.30e-01	5.78	1.31e-01	1.43	6.00e-02	0.65
31841	5.00e-02	2.76e-01	5.52	7.11e-02	1.42	3.23e-02	0.65
241857	2.76e-02	1.43e-01	5.17	3.89e-02	1.41	1.75e-02	0.63

$\|\nabla u\|^2 = 0.397882$. As before, we compare the three types of estimators SEE, HEE and CEE. Locally refined mesh are shown in Figure 7. SEE leads to a stronger refinement at the inner corner, whereas HEE and CEE lead to finer cells close to the adjacent edges too.

In Table 3 we list the obtained values for this 3D example on equidistant tensor meshes. The efficiency indices stabilize for the three methods but at different values. The standard error estimator SEE settle at a value of approximately 5, the higher-order estimator HEE level out at 1.4 and the cheaper version CEE at about 0.63. On locally refined meshes (Table 4) all considered types of estimators show a slight increase of the efficiency index. We observed this phenomena also in the previous 2D example. This is probably due to the presence of hanging nodes on the hexahedral meshes. However, the increase is very moderate. The effectivity index of SEE is once again the worsest one (I_{eff} is approaching nearly 8). HEE overestimates the error by a factor of 2 on very fine meshes, and CEE ends by a factor of 0.95 on the finest mesh with about 2.4 million mesh points.

Finally, we show in Figure 8 the development of the error in dependence of the number of mesh points for global and local refinement. Although the obtained meshes are different in dependence of the used estimation technique (Figure 7), the performance is very similar and very good in comparison to global refinement.

References

[1] M. Ainsworth and J. T. Oden. A unified approach to a posteriori error estimation using element residual methods. *Numer. Math.*, 65(1):23–50, 1993.

[2] M. Ainsworth and J. T. Oden. *A Posteriori Error Estimation in Finite Element Analysis.* Wiley Interscience, New York, 2000.

[3] I. Babuska and W. C. Rheinboldt. Error estimates for adaptive finite element computations. *SIAM J. Numer. Anal.*, 15:736–754, 1978.

TABLE 4. Obtained efficiency indices in 3D with estimators SEE, HEE and CEE on locally refined meshes.

SEE		HEE		CEE	
#nodes	I_{eff}	#nodes	I_{eff}	#nodes	I_{eff}
31841	5.52	31841	1.42	31841	0.65
36699	6.29	40057	1.53	40385	0.71
38337	6.44	48453	1.58	257019	0.71
277047	6.44	300307	1.63	321947	0.78
300705	6.98	336417	1.67	2026801	0.86
2181725	7.82	2273981	1.93	2481819	0.95

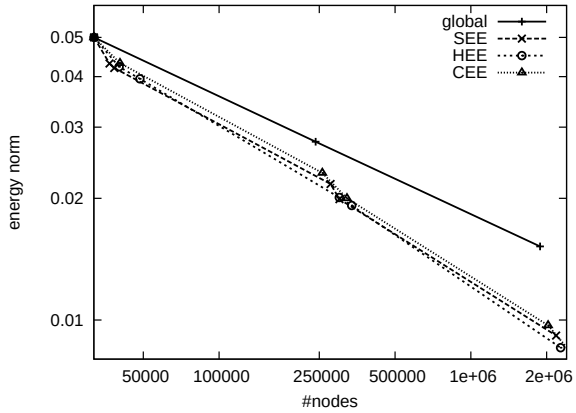

FIGURE 8. Comparison of the energy error in 3D for global and local refinement in dependence of the number of nodes.

[4] R.E. Bank. Hierarchical bases and the finite element method. *Acta Numer.*, 44:1–43, 1996.
[5] R. Becker and R. Rannacher. An optimal control approach to a posteriori error estimation in finite element methods. *Acta Numer.*, 10:1–102, 2001.
[6] M. Braack, E. Burman, and B. Taschenberger. Duality based a posteriori error estimation for quasi periodic solutions using time averages. *SIAM J. Sci. Comput.*, 33:2199–2216, 2011.
[7] C. Carstensen and R. Verfürth. Edge residual dominate a posteriori error estimates for low order finite element methods. *SIAM J. Numer. Anal.*, 36(5):1571–1587, 1999.
[8] W. Dörfler. A convergent adaptive algorithm for Poisson's equation. *SIAM J. Numer. Anal.*, 33(3):1106–1124, 1996.
[9] Th. Richter. Parallel multigrid for adaptive finite elements and its application to 3D flow problem. PhD Dissertation, Universität Heidelberg, 2005.
[10] I. Babuška and T. Strouboulis. *The Finite Element Method and its Reliability.* Oxford Univers. Press, 2001.
[11] R. Verfürth. A posteriori error estimates for nonlinear problems. finite element discretization of elliptic equations. *Math. Comput.*, 62:445–475, 1994.
[12] R. Verfürth. *A Review of A Posteriori Error Estimation and Adaptive Mesh-Refinement Techniques.* John Wiley/Teubner, New York-Stuttgart, 1996.
[13] D. Yu. Asymptotically exact a posteriori error estimators for elements of bi-even degree. *Chinese J. Num. Math. and Appl.*, 13:82–90, 1991.
[14] D. Yu. Asymptotically exact a posteriori error estimators for elements of bi-odd degree. *Chinese J. Num. Math. and Appl.*, 13:64–78, 1991.

Mathematisches Seminar, Christian-Albrechts-Universität zu Kiel, Ludewig-Meyn-Str. 4, D-24098 Kiel, Germany

E-mail: braack@math.uni-kiel.de and taschenberger@math.uni-kiel.de